Core-electron spectra and electronic structure of $CeNbS_3$

Youichi Ohno
Department of Physics, Faculty of General Education, Utsunomiya University, 350 Mine-machi, Utsunomiya 321, Japan
(Received 16 December 1992; revised manuscript received 8 March 1993)

Core-electron-spectroscopy studies have been made for $CeNbS_3$, which is one of the misfit-layer compounds. The Ce $3d$ and $4d$ x-ray photoemission (XPS) spectra are quite similar to those in CeSe. Ce exists mainly as a trivalent ion and the $4f$ electrons hybridize with other conduction and valence electrons. The S $2p$ XPS spectrum exhibits only a broad peak which consists of plural spin-orbit-split structures at different chemical environments. We find some evidence which indicates interlayer interaction and electron transfer from the Ce $5d$ band to the Nb d_{z^2} band. The Nb $N_{2,3}$ inner-shell-electron energy-loss spectrum exhibits a small peak just above the threshold, indicating that the d_{z^2} band is still incompletely filled after charge transfer. The overall structures of the conduction band and interband transitions are understood in terms of the electronic structure of each layer. Preferential plasma excitation has also been discussed.

I. INTRODUCTION

$CeNbS_3$ is a misfit-layer compound in which CeS and NbS_2 layers are alternately stacked along the c axis. The crystal structure consists of two different types of orthorhombic unit cells mismatched along the a axis.[1] It is shown schematically in Fig. 1. The CeS layer has a C-centered orthorhombic unit cell and the atomic arrangement closely resembles that of a rocksaltlike lattice sliced perpendicularly to the $\langle 001 \rangle$ direction by two planes with an interplanar distance of half the lattice constant. The dimension of the unit cell is given by the parameters $a_1=5.727$ Å, $b_1=5.765$ Å, and $c_1=11.41$ Å. The NbS_2 layer has an F-centered orthorhombic unit cell. The atomic arrangement is the same as that of pure NbS_2 in which Nb atoms are surrounded by a trigonal prism of six S atoms. The lattice constants are $a_2=3.311$ Å, $b_2=5.75$ Å, and $c_2=22.82$ Å. Since both unit cells contain four molecules, the exact chemical composition is given by the chemical formula $(CeS)_{1.16}NbS_2$.

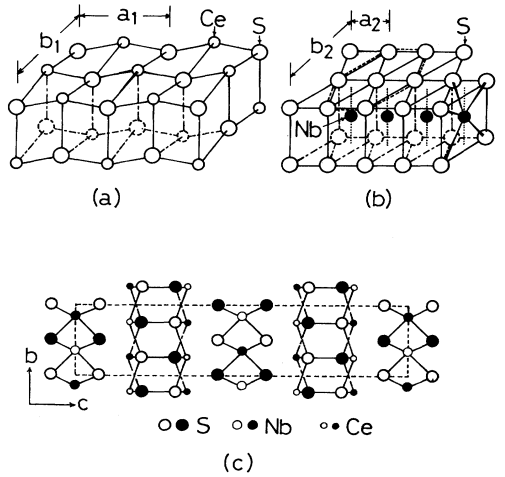

FIG. 1. Crystal structure of $CeNbS_3$: (a) CeS layer; (b) NbS_2 layer in which Nb atoms are surrounded by six trigonal prism S atoms; (c) unit cell of $CeNbS_3$ projected along the [100] axis. Open and full circles denote atoms located at $x=0$ and $x=\frac{1}{2}$, respectively.

The electrical resistivity shows a metallic behavior both in the ab plane and along the c axis.[1] The positive Hall and Seebeck coefficients mean that the dominant charge carrier is a hole. Magnetic susceptibility shows a Curie-Weiss behavior in the range of 50–300 K and a pronounced peak at 3.0 K for $H_\perp$, which is the field perpendicular to the layers.[1] The result suggests that ferromagnetically ordered Ce ions in a CeS layer are coupled antiferromagnetically with those in adjacent CeS layers. The effective magnetic moment was estimated to be $2.76\mu_B$ and $3.36\mu_B$ for $H_\parallel$ and $H_\perp$, respectively, which is slightly larger than the theoretical value of localized Ce^{3+}. Wiegers *et al.*[1] suggested that the disagreement was caused by the presence of a small amount of Ce^{2+} ions. On the other hand, Peña, Meerschaut, and Rabu[2] obtained the effective magnetic moment of $2.54\mu_B$, which was exactly predicted from Ce^{3+}.

Bulk CeS exhibits metallic properties, exciting an electron per Ce atom into the conduction band. Croft and Jayaraman[3] found a drastic change in volume with no change in crystal structure at a pressure of about 12.5 GPa. This change implies that the valence transition occurs in Ce by intersecting the $4f$ levels with the conduction band. The photoemission result of Croft *et al.*[4] shows that the Ce $4f$ band, which contains little S $3p$ character, is located in the energy gap between the Ce $5d$ conduction band and the S $3p$ valence band, in agreement with the Koringa-Kohn-Rostoker band calculation.[5] On the other hand, Vedel *et al.*[6] found only a continuous volume variation up to 25 GPa, and the self-consistent linear augmented plane-wave band calculation[7] in the local-density approximation shows a large overlap of the $4f$ states with the conduction-band states near the Fermi level. No theoretical and experimental studies on electronic structure have been carried out for $CeNbS_3$ until now.

A previous core-electron x-ray photoemission spectro-

scopy (XPS) study[8] has shown that valence mixing is small in $SmNbS_3$ akin to $CeNbS_3$ even if it occurs. Sm exists mainly as a trivalent ion in contrast with bulk SmS in which Sm exists as a divalent ion. It has been considered that the valence transition from divalency to trivalency results from electron transfer from SmS layers to NbS_2 layers. Sm $3d$ and $4d$ core electrons and valence-band XPS spectra give direct information on the number of $4f$ electrons and valence fluctuations such as this. This is due to the following fact: Sm $4f$ electrons are spatially localized, so that a strong Coulomb interaction with a core hole shifts the $4f$ levels downward in energy below the Fermi level. However, electron transfer from ligands, that is, the shake-down process, does not occur because of negligibly small coupling with ligand orbitals. Then, the number of $4f$ electrons remains unchanged. In this case, core-electron spectra reveal only a peak. In the case of Ce alloys and compounds, the radial wave functions of Ce $4f$ electrons extend over the region of ligand valence electrons, which results in mixing between the orbitals and makes the shake-down process possible. As a result, the core-electron spectra reveal two peaks corresponding to two different final-state configurations, that is, a poorly screened final state and a well-screened final state. This final-state effect plays an important role for the XPS and x-ray-absorption spectroscopy (XAS) spectra and prevents a direct quantitative determination of the number of $4f$ electrons. With the aid of theory based on the Anderson impurity model, however, we can give information on it from the core-electron-spectroscopy studies.

This paper presents the core-electron-spectroscopy study of $CeNbS_3$. In Sec. III A the Ce $3d$ and $4d$ and the S $2p$ XPS spectra are presented. In this section we discuss the number of $4f$ electrons and their hybridization with other electrons, comparing them with the $3d$ and $4d$ XPS spectra of other Ce compounds and with the theoretical calculations of Gunnarsson and Schönhammer[9,10] and Kotani and co-workers[11,12] based on the Anderson impurity model. We also discuss the interlayer interaction in relation to the chemical shift of the S $2p$ peaks. In Sec. III B the x-ray-absorption spectroscopy and the inner-shell electron energy-loss spectroscopy (ISEELS) results are presented. From near-edge structures we discuss charge transfer from CeS layers to NbS_2 layers. In Sec. III C the valence-band reflection-electron energy-loss spectroscopy (REELS) results are presented. In this section we discuss interband transitions and preferential plasma excitation.

II. EXPERIMENT

Single crystals of $CeNbS_3$ were grown using the chemical-vapor-transport reaction in a silica ampoule which was evacuated and then sealed. The following reaction has been completed in the ampoule:

$$\tfrac{1}{2}Ce_2S_3+(1-x)Nb+x\,NbCl_5+\tfrac{3}{2}S\rightarrow CeNbS_3+\tfrac{5}{2}x\,Cl_2\ , \quad (1)$$

where $x=0.05$. On the right-hand side, the resulting Cl_2 was employed as a transport agent. Crystal-growth conditions such as a temperature gradient were the same as those of $SmNbS_3$.[8] After a month, large thin crystals with a diameter of about 7 mm were grown in the high- and intermediate-temperature zones. Atomically clean and smooth surfaces were prepared by cleaving with adhesive tape in the atmosphere just before the measurements. Auger electron spectroscopy spectra and core XPS spectra displayed small carbon and oxygen contaminant peaks, but the argon-ion-sputtering technique combined with the annealing technique, which was customarily used for surface cleanness, was not employed, because it produced atomic disorder and deviation from stoichiometric chemical compositions at the surface and because the cleaved surfaces were very stable chemically and structurally, reflecting the two-dimensional crystal structure.

The Ce $3d$ and $4d$ and the S $2p$ XPS spectra were measured with unmonochromated Mg and Al $K\alpha$ radiation, the excitation energies being 1253.6 and 1486.6 eV, respectively. Emitted photoelectrons from a surface were analyzed in energy with a double-pass cylindrical mirror analyzer (CMA) (Perkin-Elmer Instruments, model 15-255G). The binding energies were corrected, employing the Cu $2p_{3/2}$ (932.4 eV) and Cu $3s$ (121.4 eV) lines and the contaminant C $1s$ (284.6 eV) line as reference lines. A vacuum system and a data-acquisition and processing system were the same as those in REELS. The Ce $N_{4,5}$ ISEELS spectrum and the valence-band REELS spectrum were measured with a normal-incidence electron gun coaxial to the CMA. They were represented as an energy distribution curve or, in the second-derivative form, using a lock-in amplifier. Our REELS apparatus and data-acquisition and processing system have been described in a previous paper.[13]

The Nb L_2 and S K XAS spectra of $CeNbS_3$ and NbS_2 were measured with a Johan-type vacuum soft-x-ray spectrometer with a Rowland circle of radius 30 cm. The description of our XAS apparatus and data-acquisition and processing system has been made in a previous paper.[14] The difference spectrum was obtained by subtracting the normalized optical density of NbS_2 multiplied by an adjustable parameter from the normalized optical density of $CeNbS_3$. This parameter was determined, assuming that both spectra have the same optical density at the Nb L_2 peak.

III. RESULTS AND DISCUSSION

A. XPS results

The XPS technique is a powerful means for investigating the valence fluctuation in the mixed valence systems involving Sm and heavier rare-earth metals as described above.[15] However, in the core-electron-spectroscopy studies of Ce metal, alloys, and compounds, the final-state effect, which arises from the interconfiguration interaction in the presence of a core hole, is more important due to the hybridization of $4f$ electrons with other conduction electrons and/or valence electrons, and the direct determination of the number of $4f$ electrons be-

comes difficult. For example, in the Ce $3d$ XPS spectra of typical trivalent compounds such as CeF_3, two peaks corresponding to a well-screened $3d^9 4f^2 v^{m-1}$ final state and a poorly screened $3d^9 4f^1 v^m$ final state are observed. Here, v represents the valence electrons. In mixed-valent compounds, we can observe a peak corresponding to the $3d^9 4f^0$ final state in addition to the peaks.

A decade ago Gunnarsson and Schönhammer[9] calculated the Ce $3d$ XPS spectra as functions of $P(f^0)$, the probability of having no f electrons in the initial state and Δ, the charge-transfer energy which depends on the hybridization between the f states and the conduction- or the valence-band states. According to the calculation $w(f^0)$, the weight of the $3d^9 4f^0$ peak, in other words, the intensity of the $3d^9 4f^0$ peak relative to the total intensity, almost agrees with the value of $P(f^0)$ although the disagreement cannot be neglected, particularly in the small $P(f^0)$ region. In XPS, it is slightly smaller than $P(f^0)$. $r(I_{f^2}/I_{f^1})$, the intensity ratio of the f^2 to the f^1 peak, on the other hand, strongly depends on Δ and $P(f^2)$, the probability of having two f electrons in the ground state. This value increases with Δ owing to the shake-down process. The $P(f^2)$ value is, in general, quite small. It is less than about 0.05. However, it has great influence on the intensity of the f^2 peak. The first application of the theoretical results has been done by Fuggle *et al.*,[16] to study the Ce $3d$ XPS spectra of various Ce intermetallic compounds, in which they have shown that the XPS experimental studies combined with the above calculation still provide valuable information about n_f, the number of f electrons in the initial state and Δ. Here we have attempted to apply it to the Ce $3d$ XPS spectrum in $CeNbS_3$.

The measurements of the Ce $3d$ XPS spectra of different mean free paths have been done with Mg and Al $K\alpha$ radiations. The higher spectrum in Fig. 2 has been measured with Mg $K\alpha$ radiation. Although it is more sensitive to the surface than the lower spectrum, both spectra are quite similar. This fact suggests that surface effects play only an unimportant role. The main peaks of the spin-orbit-split $3d_{5/2}$ and $3d_{3/2}$ parts, which are centered at 885 and 904 eV, respectively, are assigned to the poorly screened $3d^9 4f^1 v^m$ final state. The well-screened $3d^9 4f^2 v^{m-1}$ final state gives a shoulder at 4.0 eV below the main peaks. It is predicted from the experimental result of CeN,[17] one of the mixed-valent compounds, that a peak corresponding to the $3d^9 4f^0 v^{m+1}$ final state appears around 11 eV above the main peak. In the present case, however, the intensity is too small to distinguish it from the inelastic-scattering background. Then we may consider that the Ce^{4+} $4f^0$ configuration is less than a few percent of the ground state. The overall structures are quite similar to those of typical trivalent compounds such as CeSe,[18] CeSb,[19] and CeP.[19] The energies of the main features are tabulated in Table I. Since the f^1 and f^2 peaks are spread by exchange interaction between a core hole and localized $4f$ electrons, the area ratio of the f^2 peak to the f^1 peak $r(S_{f^2}/S_{f^1})$ provides a better measure for estimating Δ rather than $r(I_{f^2}/I_{f^1})$. However, it was difficult to decompose the peaks into each peak.

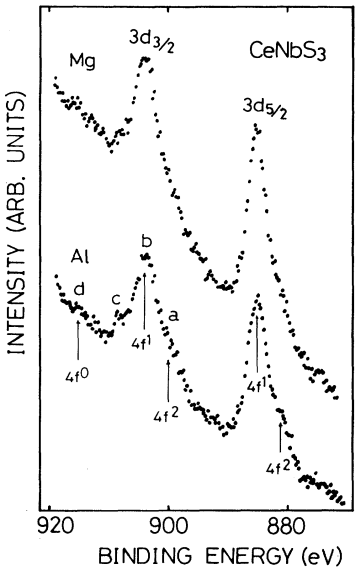

FIG. 2. Ce $3d$ XPS spectra of $CeNbS_3$ measured with Mg and Al $K\alpha$ radiations.

Then we have estimated it from $r(I_{f^2}/I_{f^1})$, following Fuggle *et al.* It was 0.1 eV, which gave an intermediate coupling strength nearly equal to that of Ce_3Pd_5.[16]

Here, we discuss the difference in the hybridization of $4f$ electrons between CeS and CeP. The valence photoemission spectrum of CeS (Ref. 4) shows a resonance behavior similar to that of the systems in which hybridization is less important. The Ce $4f$ band lies in the energy gap between the Ce $5d$ conduction band and the S $3p$ valence band. The spectrum of CeP, on the other hand, shows a strongly coupled resonance behavior and the Ce $4f$ states form a valence band just below the Fermi level with hybridization with Ce $5d$ and P $3p$ states.[4] Such a difference in hybridization between the compounds would cause dissimilar Ce $3d$ XPS spectra. However, the experimental spectra are quite similar as discussed above. Where does the discrepancy come from? Until now, Ce in a solid has been treated as a trivalent or a tetravalent ion. This is due to the fact that Ce^{2+} has a much higher excitation energy as compared to Ce^{3+} and Ce^{4+}. If we assume different $P(f^2)$ values for the CeS layer in $CeNbS_3$ and CeP, the discrepancy is solved satisfactorily within the Anderson impurity model. In fact, if we assume a larger, but less than $0.05P(f^2)$ value for the CeS

TABLE I. Energies in eV of the main features of the Ce $3d$ and $4d$ XPS spectra of $CeNbS_3$. The energies of Cu $2p^{3/2}$ and Cu $3s$ reference lines are 932.4 and 121.4 eV, respectively.

Notation	$3d^{5/2}$	$3d^{3/2}$	$4d$
a	881.0	900.0	106.8
b	885.0	904.0	109.2
c	887.5	908.0	110.4
d		915.0	111.4
e			114.2

layer, both experimental results are consistent. This assumption is partially supported by the magnetic and electrical studies of Wiegers *et al.*[1] in which they have suggested that 20% Ce^{2+} ions exist in $CeNbS_3$. If not, we should consider a change of electronic structure from that of bulk CeS. In this case, the Ce $4f$ states in $CeNbS_3$ are required to be mixed more strongly with other valence- and conduction-band states. As far as the present authors know, there are no available Ce $3d$ and $4d$ XPS spectra in CeS. The Ce $4d$ spectrum in Ce_2S_3 has been measured by Kačiulis, Letišenka, and Plešanovas.[20] It is similar to ours, although the binding energy is smaller by about 2 eV.

Figure 3 shows the Ce $4d$ XPS spectrum in $CeNbS_3$. The spectrum is explained in terms of the multiplet structures of the Ce^{3+} $4d^9 4f^1$ final state which has been calculated by Signorelli and Hayes.[21] However, it is complicated by the spin-orbit (s.o.) interaction and the interconfiguration interaction. The s.o. splitting of the Ce $4d$ levels has been estimated from the XPS spectrum of CeN (Ref. 17) to be 3.3 eV, almost in agreement with the energy distance between peaks *a* and *c*. Peak *a* might be assigned to one of the $4d^9 4f^1$ multiplet structures. However, considering the fact that peaks *a* and *c* are varied with chemical environments and that the latter peak appears in the low-density region of the calculated multiplet structures, it would be more reasonable to assign the peaks to the structures of the poorly screened $4d^9 4f^2$ final state.

Figure 4 shows the S $2p_{3/2}$ and $2p_{1/2}$ XPS spectra of various misfit-layer compounds and SnS. The s.o. splitting of about 1.2 eV and the statistical intensity ratio of 2:1 are confirmed for SnS. For the misfit-layer compounds, however, we find divergences from the values and the XPS spectrum reveals only a broad peak for $CeNbS_3$ and $SmNbS_3$. This is due to different chemical environments of the *S* atoms. Within a TS_2 layer, S $3p$ orbitals are strongly hybridized with metal *d* orbitals to form strong bonds with three *T* atoms, while within a *MS* layer they are less hybridized with valence orbitals of the surrounding five *M* atoms, especially in rare-earth compounds. The difference in chemical environments leads to multiple peaks due to the chemical shift. Here, we note some experimental results implying the difference in the interlayer interaction between the rare-earth compounds and Sn and Pb compounds. Wiegers *et al.*[1] have shown that the CeS lattice is modulated strongly along the *a* axis. The shortest interlayer atomic distance between *M* and *S* is smaller than the shortest intralayer *M-S* distance, unlike Sn and Pb compounds. Another experimental result is given from Raman-scattering experiments.[22] The spectra consist mainly of intralayer vibration modes of individual layers. For Sn and Pb compounds, Raman shifts in the NbS_2 part are quite similar to those for the pyridine-intercalated derivative and the peaks in the *A*-type mode in which *S* atoms are displaced perpendicular to the basal plane, shift to a negative direction. For rare-earth compounds, on the other hand, they shift to a positive direction. Until now, the relationships between the Raman shift, the interlayer *M-S* distance, and the chemical shift are not clear, but we may suggest at least that the interlayer interaction and chemical environments of *S* atoms are different between the compounds. Further studies are needed to make the relationships clear.

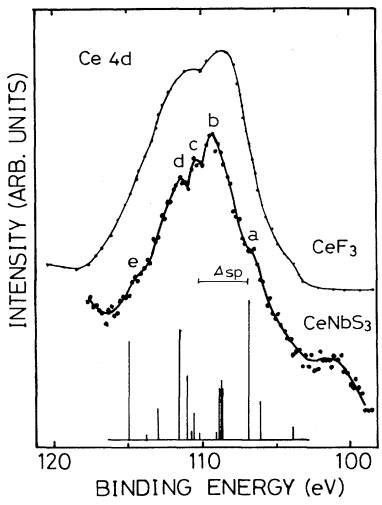

FIG. 3. Ce $4d$ XPS spectrum of $CeNbS_3$ measured with Mg $K\alpha$ radiation, which is compared with that of CeF_3 and the multiplet structures of the $4d^9 4f^1$ final state (Ref. 21). Δ_{sp} denotes the spin-orbit splitting of the Ce $4d$ levels.

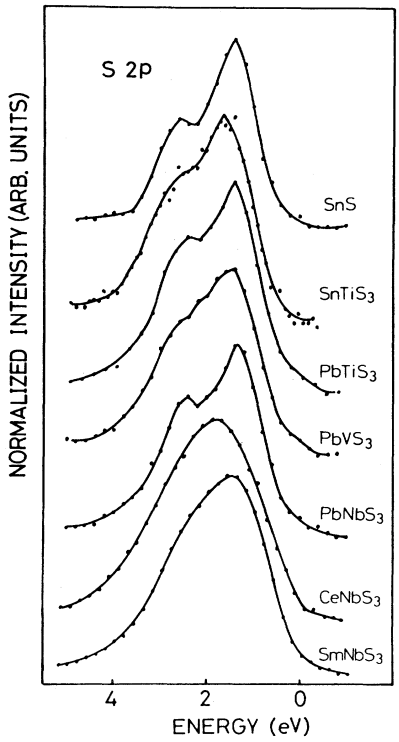

FIG. 4. S $2p$ XPS spectra of various misfit-layer compounds and SnS. Pass energy applied to CMA is 10 eV for $PbVS_3$, 15 eV for SnS and $PbTiS_3$, and 25 eV for the other compounds.

B. XAS and ISEELS results

The Ce 4*d* XAS and ISEELS final states in a trivalent Ce compound have the same $d^9 4f^2$ configuration as the well-screened final state in XPS. At high incident energy, ISEELS spectra in the reflection mode are quite similar to the XAS spectra because they obey dipole selection rules. However, at low incident energy, nondipole transitions are allowed due to the breakdown of the dipole-selection rules by large momentum transfer.[23–25] Then the intensities and the shape become different from those of the XAS spectra. Figure 5 shows the second-derivative Ce $N_{4,5}$ ISEELS spectrum in $CeNbS_3$ at incident energy (E_0) of 430 eV. The threshold energy is about 118 eV. It is found that the spectrum gives remarkable intensities to prethreshold structures. They are comparable to those of giant peaks above the threshold which are some hundred times larger than those of the prethreshold structures in the XAS spectra.[26] This is due to the momentum-transfer effect. The increased intensities are caused by nonoptically transitions which are allowed by quadrupole transitions and the exchange interaction between an excited electron and an incident electron. Kalkowski *et al.*[27] have found the suppression of the structures arising from the $4f^0$ initial state. In fact, the prethreshold structures of mixed-valent compounds are quite similar to those of a typical trivalent compound such as CeF_3. Jo and Kotani[12] gave a reasonable explanation for it on the basis of the Anderson impurity model including exchange and spin-orbit interactions and showed that the suppression was caused by hybridization between 4*f* and valence electrons. Since $CeNbS_3$ is regarded as a trivalent compound, the prethreshold structures are well interpreted in terms of the multiplet structures in $4d^{10}4f^1 \rightarrow 4d^9 4f^2$ transitions without particular consideration regarding suppression. The multiplet structures were calculated by Sugar,[26] which well reproduced the XAS spectra of various trivalent Ce compounds and mixed-valent compounds. In Fig. 5 they are compared with the prethreshold structures of $CeNbS_3$ and Ce metal. The peak positions are almost in agreement, but we can find a small dissimilarity between the spectra. Since it is known that the crystal field and hybridization affect the arrangement and the intensity distribution of multiplet terms, the dissimilarity may be attributed to the effects. However, the Ce 4*d* XAS spectra of different materials are quite similar in spite of different chemical environments.[27] Then we suggest that the dissimilarity is caused by the crystal field and the hybridization effects combined with the momentum-transfer effect. Most of the prethreshold structures are derived from optically forbidden terms such as ^4G and ^4H, whereas the initial state is ^2F. Since exchange interaction between an incident electron and an excited electron enables transitions involving a change in spin multiplicity, they can be allowed by exchange interaction. This interaction is more significant for a slower incident electron and a more strongly localized target electron. As a result, ISEELS spectra are heavily affected at low incident energy. Strasser *et al.*[24] have partially confirmed it from the ISEELS spectra of Ce metal at 350 and 1595 eV.

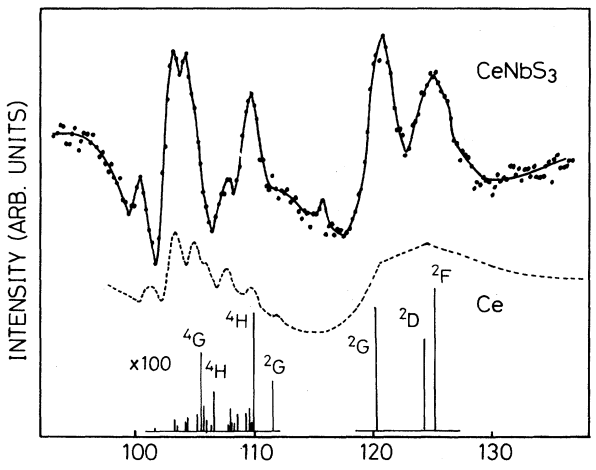

FIG. 5. Second-derivative Ce $N_{4,5}$ ISEELS spectrum of $CeNbS_3$ at $E_0 = 430$ eV in reflection geometry, which is compared with that of Ce metal (Ref. 24) at $E_0 = 350$ eV and the multiplet structures (Ref. 26) calculated for the $4d^{10}4f^1 \rightarrow 4d^9 4f^2$ transitions. The ISEELS spectrum of Ce metal is represented as an energy distribution curve as originally given by Strasser *et al.* (Ref. 24). The Ce $N_{4,5}$ threshold is located at about 118 eV.

Figure 6 shows the Nb L_2 and S *K* XAS spectra in $CeNbS_3$ and NbS_2 and the S *K* spectrum in Ce_2S_3. Unlike the Ce $N_{4,5}$ ISEELS spectrum the Nb L_2 and the S *K* spectra represent the unoccupied energy-band structures due to strong hybridization between Nb 4*d* and S 3*p* orbitals. The shoulder *a'*, which arises from the empty states of the half-filled Nb d_{z^2} band, diminishes in $CeNbS_3$. For clarity of this change, the difference spectrum is shown on the bottom of Fig. 6. It is found that large dips, which are produced by filling the Nb d_{z^2} band with electrons transferred from CeS layers, appear at the Nb L_2 and S *K* absorption edges. Such dips are observed for all the misfit-layer compounds already studied.[8,28] Then it may be considered that charge transfer is a common feature for the compounds and plays an important role for the stabilization of the crystal structure. We may discuss it theoretically by calculating the potential energy of alternatively stacking semi-infinite positive and negative thin layers. The positive part in the difference spectrum gives the contribution of S *K* absorption in CeS layers. In comparison with the S *K* spectrum in Ce_2S_3 and the partial density of S 3*p* states calculated by De and Chatterjee,[7] we find a good coincidence among the near-edge structures and the partial density of states. Since the calculation makes it clear that the first peak just above the Fermi level consists mainly of Ce 4*f* states with small S 3*p* character, we may suggest that a shoulder just above the absorption edge is derived from the Ce 4*f* band although the lowest empty states consist of Ce 5*d* states which are widely spread, having a peak 2 eV above the Ce 4*f* band. Finally, the comparison among the spectra leads to the conclusion that the peaks *b*, *d*, *g*, and *k* are

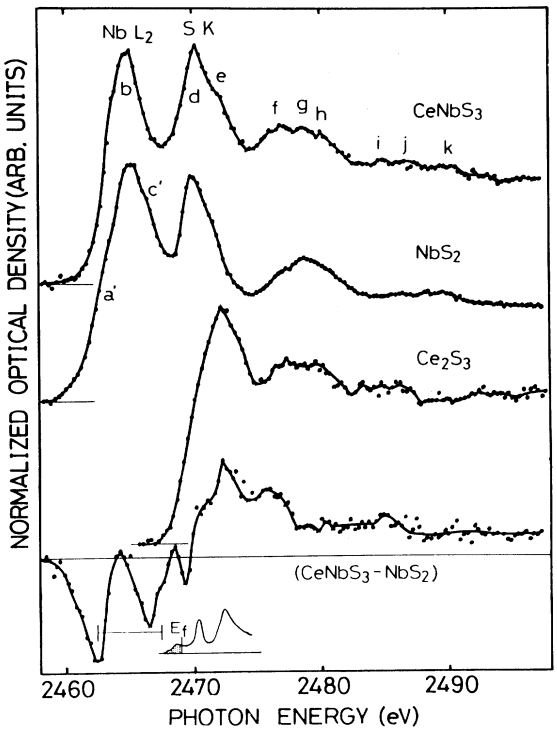

FIG. 6. Nb L_2 and S K x-ray absorption of $CeNbS_3$, compared with that of NbS_2. The lowest spectrum is the difference spectrum which has been obtained by subtracting the spectrum of NbS_2 from that of $CeNbS_3$, assuming that the optical densities are the same at the Nb L_2 peak. The positive part is compared with the S K XAS spectrum of Ce_2S_3 and the partial density of S $3p$ states of CeS (Ref. 7).

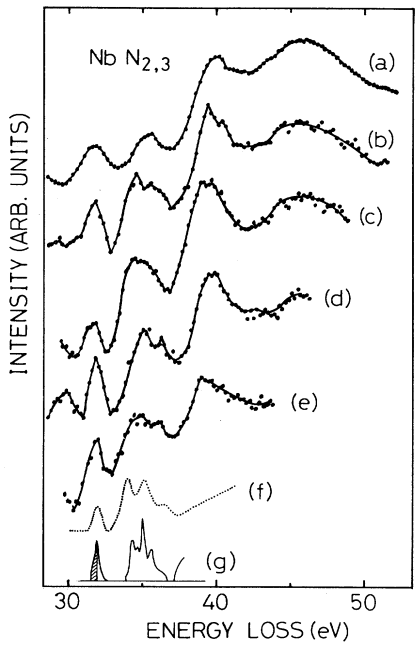

FIG. 7. Nb $N_{2,3}$ ISEELS spectra of various misfit-layer Nb compounds, which are compared with (f) the Se M_5 XAS spectrum of $NbSe_2$ (Ref. 30) and (g) the density of states of NbS_2 (Ref. 29). (a) $SmNbS_3$ at $E_0=350$ eV, (b) $SmNbS_3$ at $E_0=200$ eV, (c) $CeNbS_3$ at $E_0=200$ eV, (d) $PbNbS_3$ at $E_0=200$ eV, (e) $SnNbS_3$ at $E_0=200$ eV. The Nb $N_{2,3}$ threshold is located at 31 eV.

derived from the transitions within NbS_2 layers while the peaks e, h, and j are derived from the transitions within CeS layers and that the interlayer interaction is weak, but causes the peak f and diminishes the peaks a' and c'.

Figure 7 shows the Nb $N_{2,3}$ ISEELS spectra of various Nb misfit-layer compounds. Their spectra represent the unoccupied energy-band structures as well as the Nb L_2 and S K spectra. They are compared with the density of states calculated by Mattheiss[29] for NbS_2 and with the Se M_5 XAS spectrum measured by Sonntag and Brown[30] for $NbSe_2$. The near-edge structures of the Se M_5 spectrum arise from p states in the neighborhood of Se atoms while the Nb $N_{2,3}$ spectrum represents the d partial density of states in the neighborhood of Nb atoms dominantly. In spite of the difference, both spectra are quite similar, reflecting strong hybridization of the Nb orbitals with the chalcogen p orbitals. A peak just above the Nb $N_{2,3}$ threshold is caused by transitions to the empty states of the Nb d_{z^2} band. Then we may indicate that the d_{z^2} band is still incompletely filled after charge transfer. The area ratio of the peak to the peak arising from the remaining d bands has been estimated. It is 0.28, 0.15, 0.22, and 0.25 for $SmNbS_3$, $CeNbS_3$, $SnNbS_3$, and $PbNbS_3$, respectively. These values are larger than the expected value of 0.13 for pure NbS_2. The result is apparently inconsistent with other experimental results which suggest charge transfer from MS to NbS_2 layers. This contradiction partially comes from the lifetime broadening of a core hole and background subtraction errors. In $SmNbS_3$ the Nb $N_{2,3}$ spectrum is superimposed on the high-energy structures of the Sm $O_{2,3}$ spectrum, the threshold energy being 22 eV. The more important cause is the difference in characters between the bands. S $3p$ states are mixed more strongly with the remaining d states than the d_{z^2} states. Since the oscillator strength for an energy-loss structure is affected by band character, we should use different weights for the peaks. Nevertheless, we may suggest that the charge transfer is most prominent in $CeNbS_3$ among the Nb misfit-layer compounds.

C. Valence plasmons and interband transitions

Figure 8 shows the comparison among the EELS spectra of $SnNbS_3$, $SmNbS_3$, and $CeNbS_3$. A large peak around 20–22 eV arises from the excitation of valence plasmons. The free-electron values are calculated from the well-known relation $E_p=\hbar e\sqrt{n/\varepsilon_0 m}=37.0\sqrt{n}$ (eV), where n is the density of the valence electrons participating in plasma oscillation per unit volume ($Å^3$). They are obtained for each layer in both charged and neutral cases which depend on whether or not an electron per

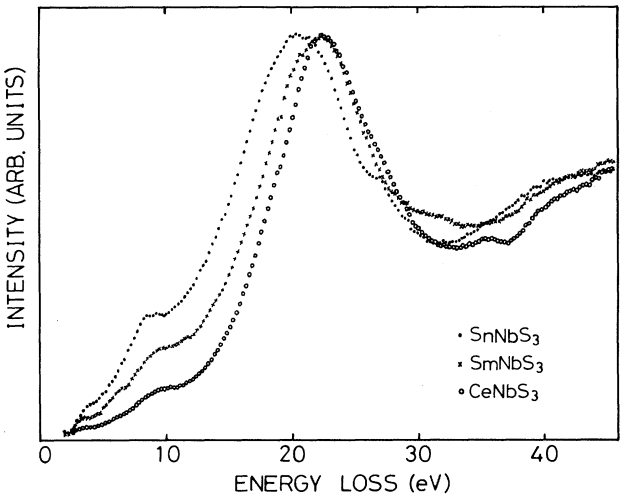

FIG. 8. Valence-electron-excited REELS spectra of $CeNbS_3$ at $E_0=1500$ eV and $SnNbS_3$ and $SmNbS_3$ at $E_0=2000$ eV.

molecule is transferred from MS to TS_2 layers. However, the charge-transfer effect on the plasma energy is not so large. Since the thicknesses of the MS and TS_2 layers are nearly equal, the free-electron value of a bulk plasmon of a misfit-layer compound is given by[31]

$$E_p=\left[\frac{[E_p(MS)]^2+[E_p(TS_2)]^2}{2}\right]^{1/2}, \quad (2)$$

where $E_p(MS)$ and $E_p(TS_2)$ are the energies of the valence plasmons of MS and TS_2 layers, respectively. The results are tabulated in Table II together with the lattice constants. Since the plasmon peaks shift to higher energy with momentum transfer, the experimental values for comparison are measured at high incident energy to neglect the momentum-transfer effect. For NbS_2 it is larger by about 2 eV than the free-electron value.[34] The disagreement is partially caused by a deviation from the simple free-electron model and is partially caused by S $3s$ interband transitions around 18 eV because plasmon peaks shift to higher energy by interband transitions on the lower-energy side. The peak energies for $CeNbS_3$ and $SmNbS_3$ are different by about 4 eV from the free-electron values of the bulk plasmons, but they are in good agreement with the experimental value of NbS_2. The peak energy for $SnNbS_3$ is, on the other hand, larger by about 2 eV than the free-electron value as well as NbS_2. Here, it is worth noting that the plasmon intensities or the oscillator strengths of M monosulfides (M=Sn, Sm, and Ce) and the sesquisulfides decrease while going from Sn to Ce compounds.[21,35] In a previous paper[31] the present author indicated the generation of interface plasmons between the layers and the possibility of preferential plasma excitation. If plasma excitation within a MS layer is much weaker than that within a NbS_2 layer, valence plasmons are excited preferentially only in NbS_2 layers. If it is comparable to that of the NbS_2 layer, interface plasmons are excited. Since the energy of the interface plasmon is given in the same form as that of the bulk plasmon given by Eq. (2), they are not distinguished only from the peak position. A detailed analysis shows that all the spectra reveal structures at 20.4 and 22.4 eV, although the intensities are very different among the compounds. We may ascribe them to the interface plasmon and the valence plasmon of the NbS_2 layer because the energy difference from the free-electron value is about 2 eV in both cases. The difference in intensity is caused by different oscillator strengths for a valence plasmon within a MS layer. Finally, we may suggest that $SmNbS_3$ and $CeNbS_3$ belong to the former case in which preferential plasma excitation occurs and $SnNbS_3$ belongs to the latter case in which interface plasmons are excited. At low incident energy, however, preferential plasma excitation occurs in $SnNbS_3$ by the momentum-transfer effect as discussed in a previous paper.[31] The difference in oscillator strengths also affect the incident-energy dependence of the observed plasmon peak and the intensities on the lower-energy side. Figure 9 shows the EELS spectra of $CeNbS_3$ at various incident energy. The incident-energy dependence is similar to those of $SmNbS_3$, layered transition-metal disulfides, and three-dimensional compounds. The plasmon peak approaches

TABLE II. Energies in eV of the bulk plasmons of $SnNbS_3$, $CeNbS_3$, and $SmNbS_3$ and the valence plasmons of individual layers in the neutral and charged cases and the lattice parameters in Å.

Material		Valence plasmon Neutral	Valence plasmon Charged	Bulk plasmon	Lattice parameter a	b	c
$SnNbS_3$	SnS	16.9	16.0		5.673	5.750	11.760[a]
				18.7			
	NbS_2	20.4	21.0		3.321	5.752	11.763[a]
$CeNbS_3$	CeS	16.2	15.3		5.727	5.765	11.41[b]
				18.6			
	NbS_2	20.7	21.3		3.311	5.765	11.41×2[b]
$SmNbS_3$	SmS	16.6	15.6		5.570	5.714	11.26×2[c]
				18.9			
	NbS_2	20.9	21.5		3.314	5.714	11.26×2[c]

[a]Meetsma *et al.* (Ref. 32).
[b]Wiegers *et al.* (Ref. 1).
[c]Meerschaut *et al.* (Ref. 33).

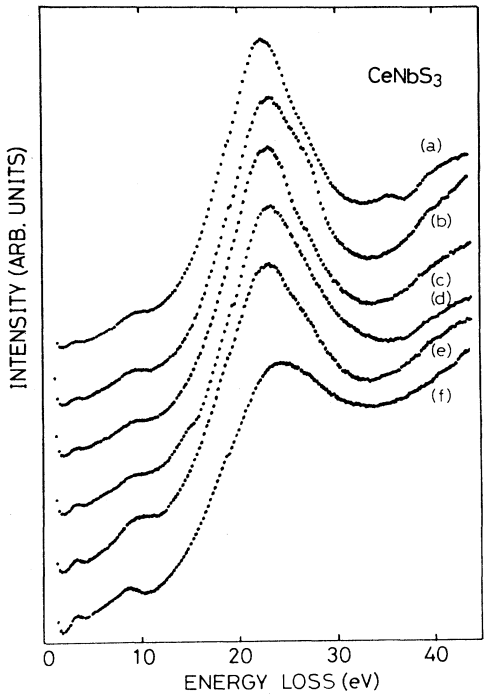

FIG. 9. REELS spectra of $CeNbS_3$ at various incident energies. (a) $E_0=1500$ eV, (b) $E_0=1250$ eV, (c) $E_0=1000$ eV, (d) $E_0=750$ eV, (e) $E_0=500$ eV, (f) $E_0=200$ eV.

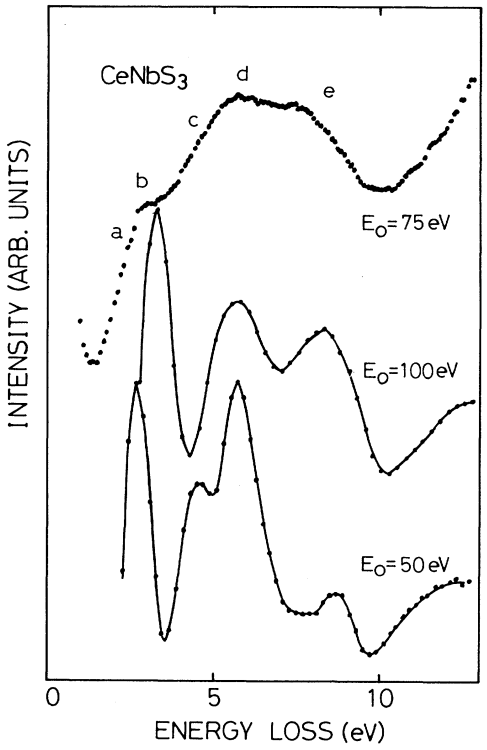

FIG. 10. REELS spectra of $CeNbS_3$ at $E_0=50$, 75, and 100 eV. The spectrum at $E_0=75$ eV has been measured in the pulse-counting mode whereas the spectra at $E_0=50$ and 100 eV have been given in the second-derivative form, using a lock-in amplifier.

a constant energy as the incident energy increases. In $SnNbS_3$ and $BiNbS_3$, on the other hand, it shifts to lower energy with incident energy almost linearly in the range of 100–2000 eV.[31]

Figure 10 shows interband transitions. The energies of the main features are summarized in Table III. Since the maximum density of states of the remaining d bands is located at about 3 eV above the Fermi level, we assign a peak at 2.7 eV to interband transitions from the d_{z^2} band to the remaining d bands. At $E_0=100$ eV its peak apparently shifts to 3.3 eV, and a peak at 4.5 eV, which may be assigned to interband transitions from the Ce $4f$ band, disappears. This is due to reduced energy resolution. In the lock-in mode, energy resolution decreases with incident energy and a primary peak covers any structures below 2.5 eV. The spectrum at $E_0=75$ eV, which has been measured in the pulse-counting mode, exhibits a fine structure at 2.2 eV. Since the optical conductivity spectrum of CeS (Ref. 36) has only small intensities in the range of 1–4 eV, we may ascribe it to interband transitions from the top of the S $3p$ valence band to unoccupied Nb d_{z^2} states within NbS_2 layers. As the incident energy decreases, a peak around 8.3 eV shifts to higher energy and the intensity decreases. This peak arises from the partial plasma resonance of Nb $4d$ electrons. Such variations are caused by the momentum-transfer effect cou-

TABLE III. Energies in eV of the main features of the EELS spectrum of $CeNbS_3$.

Notation	Energy	Assignment
a	2.2	The top of the S $3p$ valence band → unoccupied d_{z^2} states
b	2.6	Occupied d_{z^2} states → the remaining d band
c	4.5	Occupied Ce $4f$ states → the Ce $5d$ conduction band
d	5.7	The S $3p$ valence band → the Ce $5d$ conduction band within CeS layers The S $3p$ valence band → the remaining d band within NbS_2 layers
e	8.3	Partial plasma resonance of Nb $4d$ electrons

pling to the decay of plasma oscillation into single-particle excitation. The free-electron value and the observed energy of pure NbS_2 are given by Bell and Liang.[34] They are 14.7 and 8.5 eV, respectively. A broad structure around 5 eV arises from interband transitions from the S $3p$ valence band to the remaining d bands within NbS_2 layers and interband transitions from the S $3p$ valence band to the Ce $5d$ conduction band within CeS layers.

IV. CONCLUSIONS

In this paper the core-electron spectroscopy studies of $CeNbS_3$ have been presented. The Ce $3d$ XPS spectrum has been analyzed with the aid of the calculation of Gunnarsson and Schönhammer.[9] It has been found that Ce exists mainly as a trivalent ion. Ce^{2+} and Ce^{4+} are less than 5% of Ce^{3+} even if they are present. It is, however, possible that Ce $4f$ electrons are hybridized with valence and conduction electrons to the same extent as those of CeSe and CeP unlike bulk CeS. The overall structures of the Ce $3d$ and $4d$ XPS spectra are quite similar to those of CeSe. The S $2p$ XPS spectrum suggests different, plural chemical environments for S atoms. The interlayer interaction seems different between the misfit-layer compounds involving a rare-earth element and a Sn or Pb element. The second-derivative Ce $N_{4,5}$ ISEELS spectrum at $E_0=430$ eV exhibits large prethreshold structures via the momentum-transfer effect. The intensities are comparable to those of giant peaks which are hundreds times larger than those of the prethreshold structures in XAS. The Nb L_2 and S K XAS spectra give the evidence of electron transfer from CeS layers to NbS_2 layers, although the Nb d_{z^2} band is still incompletely filled after electron transfer. The Nb $N_{2,3}$ ISEELS spectrum reveals a small peak arising from the empty d_{z^2} states. The area ratio of the peak to a remaining d-band peak gives no accurate values for the number of transferred electrons, but it has been found that charge transfer is most prominent in $CeNbS_3$ among the Nb misfit-layer compounds already studied. In $SmNbS_3$ charge transfer occurs from the Sm $4f$ band, resulting in the change of the valence state from divalency to trivalency. In $CeNbS_3$ charge transfer occurs from the Ce $5d$ conduction band without changing the valence state. This is shown schematically in Fig. 11. The Ce $5d$ conduction band, as well as the occupied $4f$ band, contains an electron per molecule in bulk CeS. In forming $CeNbS_3$ a part of the conduction electrons are transferred into the Nb d_{z^2} band in a way that the electrochemical potentials or the Fermi levels in both layers come to an agreement. The wave functions of Ce $5d$ conduction electrons are not localized around Ce ions, but extend over a CeS layer. The delocalization has been confirmed for metal Ce. Then the valence state of a Ce ion is not affected by electron transfer of Ce $5d$ conduction electrons, from CeS to NbS_2 layers. Since the oscillator strength of a valence plasmon in a CeS layer is small, preferential plasma oscillation is observed even at high incident energy.

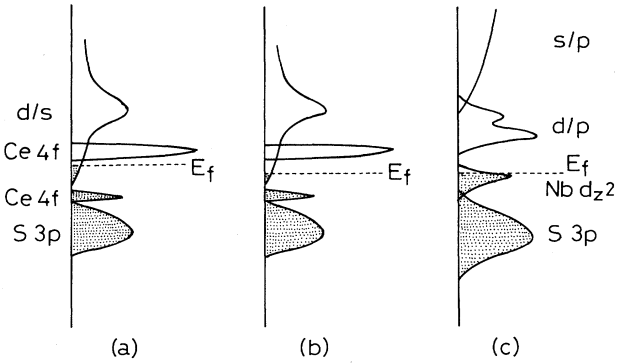

FIG. 11. Schematic energy band structure of (a) bulk CeS, (b) a CeS layer in $CeNbS_3$, and (c) a NbS_2 layer in $CeNbS_3$. In bulk CeS the Fermi level is located within the Ce $5d$ conduction band, an electron per molecule being promoted. In the CeS layer the Fermi level is lowered as the result of electron transfer to NbS_2 layers. The Nb d_{z^2} band in the NbS_2 layer is filled with transferred electrons. The overall structures of the valence and conduction bands are understood approximately in terms of the electronic structure of each layer.

[1]G. A. Wiegers, A. Meetsma, R. J. Haange, and J. L. de Boer, J. Solid State Chem. **89**, 328 (1990).
[2]O. Peña, A. Meerschaut, and P. Rabu, J. Magn. Magn. Mater. **104-107**, 1249 (1992); O. Peña, P. Rabu, and A. Meerschaut, J. Phys. Condens. Matter **3**, 9929 (1991).
[3]M. Croft and A. Jayaraman, Solid State Commun. **35**, 203 (1980).
[4]M. Croft, A. Franciosi, J. H. Weaver, and A. Jayaraman, Phys. Rev. B **24**, 544 (1981).
[5]A. V. Soldatov, A. N. Gusantinskii, and G. I. Al'perovich, Fiz. Tverd. Tela (Leningrad) **27**, 3423 (1985) [Sov. Phys. Solid State **27**, 2061 (1985)].
[6]I. Vedel, A. M. Redon, J. M. Leger, J. R. Mignod, and O. Vogt, J. Phys. C **19**, 6297 (1986).
[7]S. K. De and S. Chatterjee, Phys. Rev. B **40**, 12 304 (1989).
[8]Y. Ohno, J. Phys. Condens. Matter **4**, 7815 (1992).
[9]O. Gunnarsson and K. Schönhammer, Phys. Rev. B **28**, 4315 (1983).
[10]O. Gunnarsson and K. Schönhammer, J. Phys. (Paris) **47**, 923 (1986).
[11]A. Kotani, J. Phys. (Paris) **48**, 869 (1987); T. Nakao, A. Kotani, and J. C. Parlebas, J. Phys. Soc. Jpn. **56**, 2201 (1987).
[12]T. Jo and A. Kotani, Phys. Rev. B **38**, 830 (1988); and J. Phys. (Paris) **49**, 739 (1988).
[13]Y. Ohno, Phys. Rev. B **36**, 7500 (1987).
[14]Y. Ohno, K. Hirama, S. Nakai, C. Sugiura, and S. Okada, Phys. Rev. B **27**, 3811 (1983).
[15]M. Campagna, G. K. Wertheim, and Y. Baer, in *Photoemission in Solids II*, edited by L. Ley and M. Cardona (Springer-Verlag, New York, 1979), p. 217.
[16]J. C. Fuggle, F. U. Hillebrecht, J. M. Esteva, R. C. Karnatak, O. Gunnarsson, and K. Schönhammer, Phys. Rev. B **27**, 4637

(1983).
[17]Y. Baer and Ch. Zürcher, Phys. Rev. Lett. **39**, 956 (1977).
[18]R. Lasser, J. C. Fuggle, M. Beyss, M. Campagna, F. Steglich, and F. Hulliger, Physica **102B**, 360 (1980).
[19]Y. Baer, R. Hauger, Ch. Zürcher, M. Campagna, and G. K. Wertheim, Phys. Rev. B **18**, 4433 (1978).
[20]S. Kačiulis, A. Letišenka, and A. Plešanovas, Surf. Sci. **251/252**, 330 (1991).
[21]A. J. Signorelli and R. G. Hayes, Phys. Rev. B **8**, 81 (1973).
[22]M. Hangyo, S. Nakashima, Y. Hamada, T. Nishio, and Y. Ohno (unpublished); M. Hangyo, T. Nishio, S. Nakashima, and Y. Ohno (unpublished).
[23]F. P. Netzer, G. Strasser, and J. A. D. Matthew, Phys. Rev. Lett. **51**, 211 (1983).
[24]G. Strasser, G. Rosina, J. A. D. Matthew, and F. P. Netzer, J. Phys. F **15**, 739 (1985).
[25]Y. Ohno, Phys. Rev. B **36**, 7500 (1987); J. Phys. Soc. Jpn. **56**, 3695 (1987).
[26]J. Sugar, Phys. Rev. B **5**, 1785 (1972).
[27]G. Kalkowski, C. Laubschaut, W. D. Brewer, E. V. Sampathkumaran, M. Domke, and G. Kaindl, Phys. Rev. B **32**, 2717 (1985).
[28]Y. Ohno, Phys. Rev. B **44**, 1281 (1991); Solid State Commun. **79**, 1081 (1991).
[29]L. F. Mattheiss, Phys. Rev. B **8**, 3719 (1973).
[30]B. Sonntag and F. C. Brown, Phys. Rev. B **10**, 2300 (1974).
[31]Y. Ohno, Phys. Rev. B **40**, 1664 (1992).
[32]A. Meetsma, G. A. Wiegers, R. J. Haange, and J. L. de Boer, Acta Crystall. A **45**, 285 (1989).
[33]A. Meerschaut, C. Auriel, A. Lafond, C. Deudon, P. Gressier, and J. Rouxel, Europhys. J. Solid State Inorg. Chem. **28**, 581 (1991).
[34]M. G. Bell and W. Y. Liang, Adv. Phys. **25**, 53 (1976).
[35]R. Eymard and A. Otto, Phys. Rev. B **16**, 1616 (1977).
[36]J. Schoenes, in *Book Title,* Vol. 117 of *NATO Advanced Study Institute, Series B: Physics,* W. J. L. Buyers (Plenum, New York, 1984), p. 237.